

Machine Learning for Orders of Magnitude Speedup in Multi-Objective Optimization of Particle Accelerator Systems

Auralee Edelen¹, Nicole Neveu¹, Matthias Frey², Yannick Huber², Christopher Mayes¹, Andreas Adelmann²

¹*SLAC National Laboratory, Menlo Park, CA, USA*

²*Paul Scherrer Institut, Villigen, Switzerland*

High-fidelity physics simulations are powerful tools in the design and optimization of charged particle accelerators. However, the computational burden of these simulations often limits their use in practice for design optimization and experiment planning. It also precludes their use as online models tied directly to accelerator operation. We introduce an approach based on machine learning to create nonlinear, fast-executing surrogate models that are informed by a sparse sampling of the physics simulation. The models are $\mathcal{O}(10^6)\times$ to $\mathcal{O}(10^7)\times$ more efficient to execute. We also demonstrate that these models can be reliably used with multi-objective optimization to obtain orders-of-magnitude speedup in initial design studies and experiment planning (e.g., requiring $132\times$ fewer simulation evaluations to obtain an equivalent solution for our main test case). Our approach enables new ways for high-fidelity particle accelerator simulations to be used, at comparatively little computational cost.

Motivation

Physics simulations are essential tools for the initial design of modern particle accelerator systems, as well as for the subsequent optimization of new operating configurations. Standard codes used for this task can be computationally intensive to run. This is the case in particular when complex beam behavior must be taken into account (e.g., instabilities, collective effects, beam self-fields). Exacerbating this computational burden, accelerator systems often consist of many components that can be used to accelerate and manipulate the beam (e.g., accelerating cavities, bending and focusing magnets, collimators). Each of these components have controllable variables that can be independently adjusted to achieve specific beam characteristics. In many cases, the subtle interactions between all variables must be considered. Thus, modeling these systems from “start-to-end” (i.e., from the beginning of the accelerator to a final point of interest) is critical for obtaining realistic predictions. As a result, design and optimization studies for particle accelerator systems often require the use of thousands of cores at High Performance Computing (HPC) facilities. While in principle many large accelerator facilities have access to such resources, in practice this computational burden significantly hampers efforts to conduct comprehensive optimization studies.

Optimization studies are important in the initial design of particle accelerator systems, when many tradeoffs between possible setting combinations have to be explored. In practice, multi-objective optimization with genetic algorithms (GAs) ^{1,2} is frequently used for finding optimal setting combinations (see ³⁻⁵ for accelerator-specific examples) and examining trade-offs between achievable beam parameters (e.g., via examination of the Pareto fronts). These trade-offs drive the

selection of machine working points, which in turn guide the rest of the design process, such as selection of rf equipment.

For accelerators that are already in operation, offline optimization is also used to aid in experiment planning and setup. This is especially the case for facilities that require frequent re-tuning of settings. For example, at free electron laser (FEL) facilities like the Linac Coherent Light Source (LCLS) and Swiss Free Electron Laser (SwissFEL), user requests for specific beam parameters need to be handled quickly and efficiently, and new configurations (e.g., novel FEL schemes) are often developed during limited blocks of time between the scheduled user experiments.

Even though high-fidelity physics simulations are often created as part of the initial design process for a new accelerator, they are often not fully utilized during machine operation (i.e., as “online models”) for on-the-fly optimization and control. This again is largely due to the practical limitations related to the computational cost of these simulations: the execution speed is often too slow to aid operation. Instead, online models tend to rely on greatly simplified representations of the machine physics (e.g., see ⁶⁻⁸), and as a result trade accuracy for speed.

In light of these limitations, improving the execution speed and scalability of particle accelerator simulations is an area that has seen considerable effort in recent years ^{9,10}. Approaches to do this have focused on parallelization (e.g., see ¹¹) and hardware-based acceleration of existing simulation codes (e.g., using GPUs) ^{12,13}. In a few exceptional cases, computationally expensive models have been used to aid live operation when on-site HPC resources are available ¹⁴⁻¹⁶. Improvements to underlying modeling algorithms, such as using the Lorentz boosted frame ¹⁷ and

spectral solvers^{18,19}, have also provided orders of magnitude increases in computation speed. All of these efforts are highly successful. However, it remains the case that the computational expense of these simulations prevents them from being fully utilized by the accelerator community.

Here we explore a different, but complementary, approach that immediately enables new capabilities in how these existing high-fidelity physics simulations can be used by the particle accelerator community. We show that one can create Machine Learning (ML) based surrogate models to obtain accurate, fast-executing representations of the relevant beam dynamics from a sparse sampling of the physics simulation of interest. In contrast to the physics simulation, the ML models can execute in fractions of a second on a laptop with comparable accuracy in predicting the resultant beam parameters. We also show that these models are useful for multi-objective optimization in two important ways: (1) they can accurately reproduce optimization results obtained from the physics simulation, meaning they can be reliably used in experiment planning and live optimization during accelerator operation, and (2) they can be used to substantially speed up the initial design process by eliminating the need to run an optimization algorithm entirely on the simulation. In addition, although we do not address it in this work, these models can in principle be updated with machine measurements (e.g., see²⁰) to help improve model fidelity with respect to the real machine behavior.

We have used ML models in several previous instances to create fast-executing surrogates for computationally intensive accelerator simulations^{20–23}. Here, we build on those works, but take a substantial step forward by evaluating such models for use in optimization (and multi-objective op-

timization in particular), which is one of the main desired use-cases for ML in particle accelerator applications ²⁴. As such, this work represents an important contribution to the particle accelerator community. We also evaluate how many training samples are needed to obtain an accurate model when used for optimization and make a brief comparison between different classes of ML models.

We demonstrate the proposed approach considering two different types of accelerator systems: the injector at the Argonne Wakefield Accelerator (AWA) Facility ²⁵ (a linear accelerator) and a high-intensity cyclotron proposed for the decisive search for sterile neutrinos. The latter system is based on the Isotope Decay At Rest (IsoDAR) design, as detailed in ²⁶. The injector has a simple layout that is very similar to that used by other accelerator facilities, whereas the cyclotron is substantially more complex machine ²⁷. These two cases were chosen specifically to show the generality of the proposed approach. For simulating both accelerators, the OPAL simulation framework is used. OPAL is a parallel, particle-in-cell (PIC) code that handles nonlinear and collective beam effects (e.g., coherent synchrotron radiation, 3D space charge).

It is common practice in the accelerator community to use GAs for multi-objective optimization, although alternatives exist, such as particle swarm optimization ^{28,29}. Because of its ubiquity, we chose to run the popular NSGA-II ³⁰ algorithm with the ML models as our standard for assessing their performance. For brevity, in the subsequent text we refer to the OPAL simulation of the AWA and IsoDAR as the “physics simulation,” and we refer to NSGA-II as the “GA”.

Results

Description of ML Approach and Validation Procedure The general procedure for creating the ML surrogate models is shown in Fig. 1. An ML model is trained on a sparse random sample of the accelerator input variables and the resulting beam parameters. The ML model can then be used as a fast-executing representation of the physics simulation. To assess the performance of the ML model when used with an optimization algorithm (see Fig. 2), we run a GA with the physics simulation to optimize settings (e.g., rf cavity phases, rf cavity gradients, solenoid strengths). We then run a GA with the ML model and compare the resultant Pareto fronts. Good agreement between the Pareto fronts indicates that the ML model can be used as an accurate replacement for the physics simulation in multi-objective optimization. We also take the input points that correspond to the Pareto front from the ML model and run these through the physics simulation to check the prediction accuracy of the front.

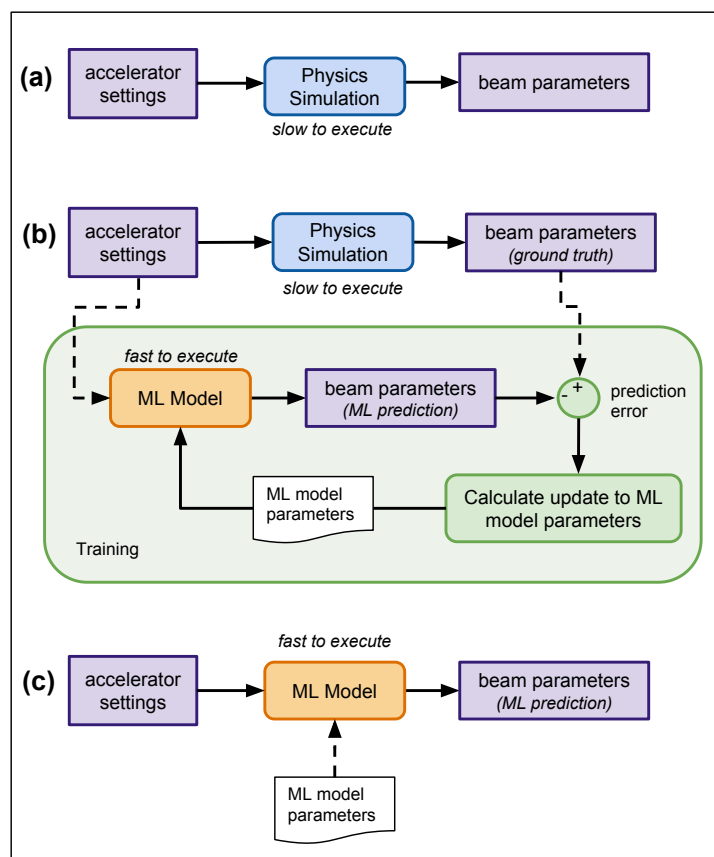


Figure 1: Initially, we have a computationally expensive physics simulation (a). We then use the physics simulation to generate a sparse set of training data for the ML model that covers a wide range of input settings. The ML model parameters are then optimized until the predictions of the beam parameters match those from the physics simulation (b). The result is a fast-executing representation of the physics simulation that can be used for optimization and online modeling (c).

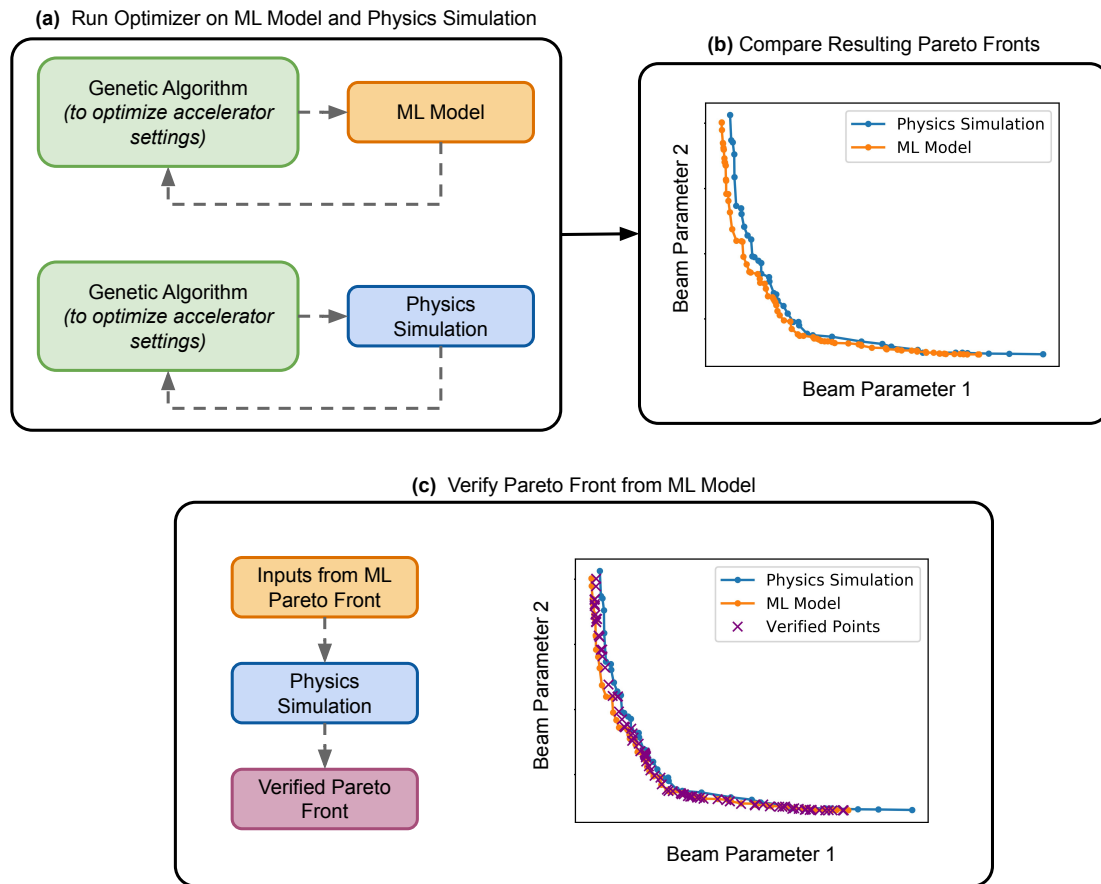


Figure 2: Approach for assessing the reliability of ML-based model when used for optimization of beam parameters. We run a GA with the physics simulation to find accelerator settings (e.g., rf cavity phases, rf cavity gradients, solenoid strengths) that optimize the beam parameters. The optimization is repeated using the ML model instead of the physics simulation. We then compare the Pareto fronts for key beam parameters. Finally, we run the inputs corresponding to the Pareto front predicted by the ML model through the simulation to verify the accuracy of the front.

Validation of ML Surrogate Modeling Approach for Optimization We chose to assess this approach first with the AWA linear accelerator. Research at the AWA is focused on advanced accelerator concepts, which generally include efforts to improve control, diagnostic instrumentation, and components (e.g., accelerating structures) for future accelerators. Much effort is also dedicated to developing and testing beamline configurations that could be used for beam shaping³¹, or future linear colliders³². Often, the accelerator settings (e.g., focusing fields for all magnets, cavity phases, cavity accelerating gradients) are adjusted prior to each experiment to achieve custom beam characteristics (e.g., bunch length and transverse sizes). The accelerator also regularly operates at bunch charges where nonlinear effects are important (e.g., 40 nC), and the cavity fields contain asymmetries. Overall, this results in a challenging optimization problem, and 3D PIC simulations are required to accurately predict the beam behavior. A fast-executing, accurate model of the machine could be useful for supporting the research program of the AWA. Taken together, these factors make the AWA a good test case.

We demonstrate the efficacy of the ML approach by training models on a sparse random sample of six adjustable input variables for the AWA and seven of the resultant beam parameters (see Fig. 3). The inputs were varied uniformly over a relevant operating range of the accelerator (see Table 3), and the same range of input variables was allowed for the GA-based optimization of the beam parameters. While the main focus was on an accelerator configuration with a bunch charge of 40 nC, we also examined a case with 1 nC bunch charge (where nonlinear effects are less important). Details on the data sets, training procedures, implementations of the ML models and the GA, and the details of the physics simulations can be found in the “Methods” section. We first

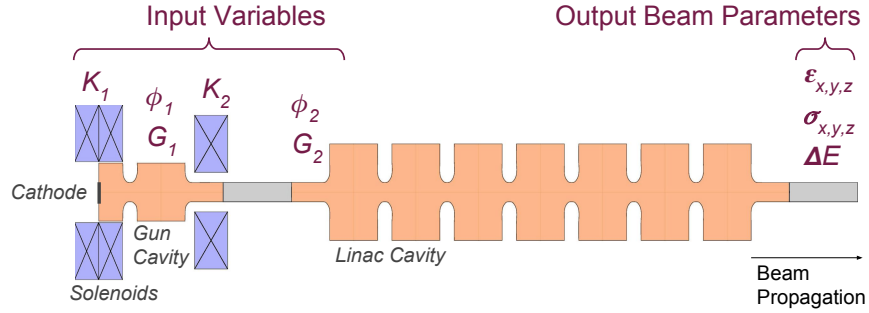


Figure 3: Schematic of the AWA linac, together with the controllable accelerator settings and predicted beam parameters. The randomly-varied inputs include the injector rf phase ϕ_1 and accelerating gradient G_1 , the linac cavity rf phase ϕ_2 and accelerating gradient G_2 , and two solenoid strengths K_1 and K_2 . The output electron beam parameters are the transverse spot sizes σ_x and σ_y , the bunch length σ_z , the transverse projected emittance values ϵ_x and ϵ_y , the longitudinal projected emittance ϵ_z , and the energy spread ΔE . The input variable ranges are determined by typical operating ranges at the AWA and are shown in Table 3. We examined this setup for 40 nC and 1 nC bunch charges.

focus on Artificial Neural Networks (NNs) to demonstrate the technique, and later briefly compare the results with those obtained from Polynomial Chaos Expansion (PCE)^{23,33} and Support Vector Regression (SVR) models.

The Pareto fronts obtained using the NN models and the physics simulation are in good agreement (see Fig. 4). Only 500 random sample points were needed to train the NN in the 40 nC case and still generate a set of Pareto fronts that is very close to those obtained with the physics simulation. In contrast, obtaining the same result with the physics simulation required 66,000

simulation evaluations. Furthermore, only a small amount of fine-tuning of the NN architecture was done in this case, as the initial topology and hyperparameters were chosen based on previous experience of the authors with similar types of injector modeling problems^{20–22}. This highlights the generality of this approach for common kinds of accelerator components and hints at the possibility for doing transfer learning with the produced models.

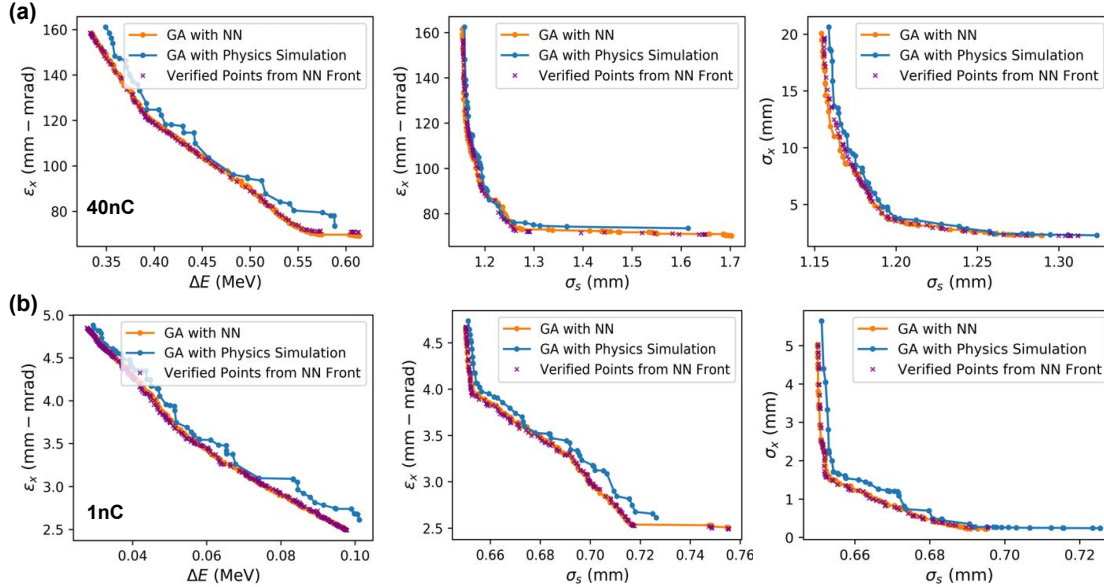


Figure 4: Comparison between Pareto fronts obtained from the NN and the physics simulation for three sets of beam parameters. We show results at the 40 nC bunch charge (a) and at the 1 nC bunch charge (b) configurations, and we find excellent agreement between the Pareto fronts. Note that while we only show three of the most important Pareto fronts, in total seven beam parameters have been optimized, making up the larger front from which these 2D fronts are projected.

In order to visualize the extent to which the NN is generalizing to new regions of the parameter space (as opposed to just learning the Pareto front directly from the training data), we compared the sampled points with the final Pareto fronts obtained with the NN (see Fig. 5). From this we see

that for some beam parameter combinations, the Pareto front is in a region of the parameter space that is not directly sampled in the training data. This indicates that the NN is able to interpolate in the parameter space of the training data (6 input dimensions, 7 output dimensions) and find better combinations of beam parameters than those observed in the training set.

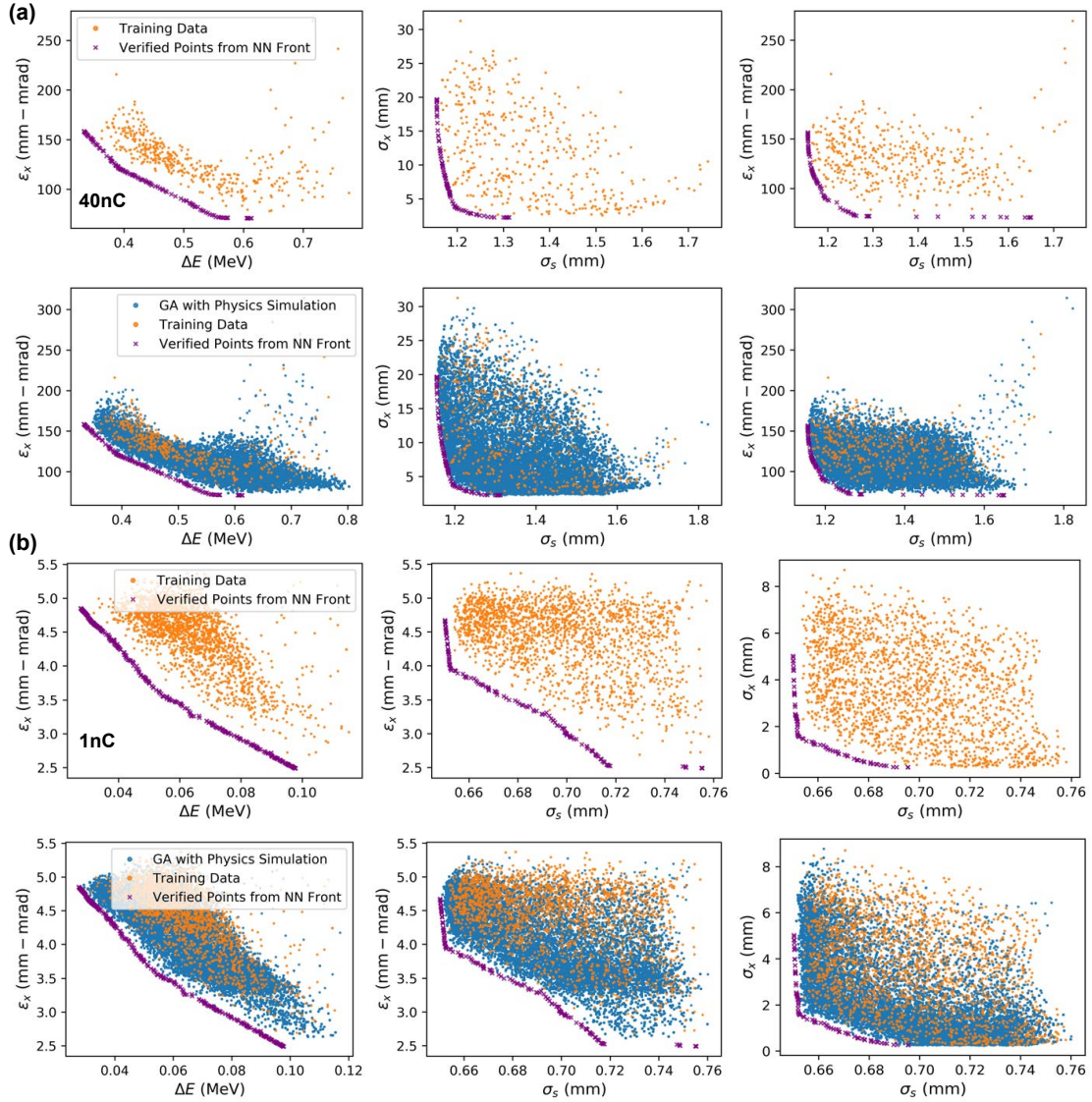


Figure 5: Visualization of improved solution found with optimizing on the NN model, as compared with the training set and the points sampled with the GA. The position of the front indicates that the NN is able to interpolate in the input space to produce better combinations of output parameters than are observed in the training data. We show the sampled points in training set and corresponding verified Pareto front from the NN for 40 nC (a) and 1 nC (b). For comparison, we also show the points sampled by the GA that was run on the physics simulation.

Impact of Training Sample Size Producing training data using the physics simulation is computationally expensive. In light of this, one question which arises is how the accuracy of the ML model will change with the number of samples used in training. This is important for estimating the corresponding trade-off between computation time needed to generate the training set and the resultant model accuracy (the requirements for which may vary depending on the application).

To address this, we trained models using 5k, 500, 200, and 100 randomly-sampled points and compared the resulting Pareto fronts obtained (see Fig. 6). Note that when using only 500 points, we do not see substantial reduction in the Pareto front accuracy. For training with 200 points, the prediction starts to deviate substantially from the ground truth, but the solution could still be used as a 'warm start' for subsequent fine-tuning with the physics simulation.

We also trained the NN models on a larger range of training sample sizes and evaluated their performance in predicting the points obtained from running the GA with the physics simulation. We quickly see diminishing returns in improvement for the prediction task after the number of samples increases beyond a few thousand (see the Supplemental Material for more details).

Improvement in Computational Efficiency by Using ML Model Once training is completed, one NN model evaluation can be computed in < 1 ms on one core of a *laptop computer*, compared with 590 seconds for one physics simulation on 8 cores for the 40 nC simulation. In Table 1, the time-to-solution and computing resources needed for the GA optimization with the physics simulation are compared with those needed for GA optimization with the NN surrogate model. The NN-based GA takes about 2 minutes on a laptop computer, which corresponds to $\mathcal{O}(10^6) \times$

fewer computing resources (in terms of core-hours) than the same optimization when conducted with the physics simulation directly.

Importantly, the overall improvement is still substantial when considering the computation time required to generate the training data and to train the NN, this makes the approach a viable way of speeding up initial design optimization. To generate enough training data to produce an accurate Pareto front in the 40 nC case, $132\times$ fewer simulation evaluations and $144\times$ fewer total core hours were required than if we were to use the physics simulation alone. Finally, the NN training itself takes approximately 10 minutes on one core of a laptop. Furthermore, for a given problem, this step of generating the data and training the model only needs to be done once, and the NN model can be used for subsequent modeling and optimization tasks (including serving as a fast stand-in for part of a larger start-to-end simulation of the full machine).

When considering the reduction in computational resources used, it is important to note that the physics simulation had already been tuned for a high level of computational efficiency. As such the results represent improvement over the state-of-the-art. We conducted massively parallel physics simulations with OPAL, which has been optimized for HPC systems, and we also use an implementation of the GA that is specifically designed to be efficient to run in parallel with OPAL. In cases where codes are less efficient or higher complexity, the ML-based approach may actually enable larger optimization studies to be conducted than would have been feasible using the physics simulation alone.

Method	Calculation	Core-hours	Wall time (hours)	Evaluations
Physics Sim.	GA on OPAL	95,000	36	65,929
ML-based	Generate training data	660	0.33	500
	GA on NN	0.03	0.03	65,600
	<i>Speedup - training included</i>	<i>144×</i>	<i>109×</i>	<i>132×</i>
	<i>Speedup - training excluded</i>	<i>3·10⁶×</i>	<i>1200×</i>	<i>n.a.</i>

Table 1: Comparison of computing resources: core-hours, wall time, and number of simulation evaluation required for running the GA with the physics simulation and the GA with the NN. Here we show only the 40 nC bunch charge, but details on 1 nC bunch charge can be found in the Methods section. When running the same GA with the NN, $3 \cdot 10^6 \times$ fewer computing resources are required. When including the resources needed to generate the training data (as might be done for initial design optimization), we still have a factor improvement of $144 \times$ in terms of core-hours required.

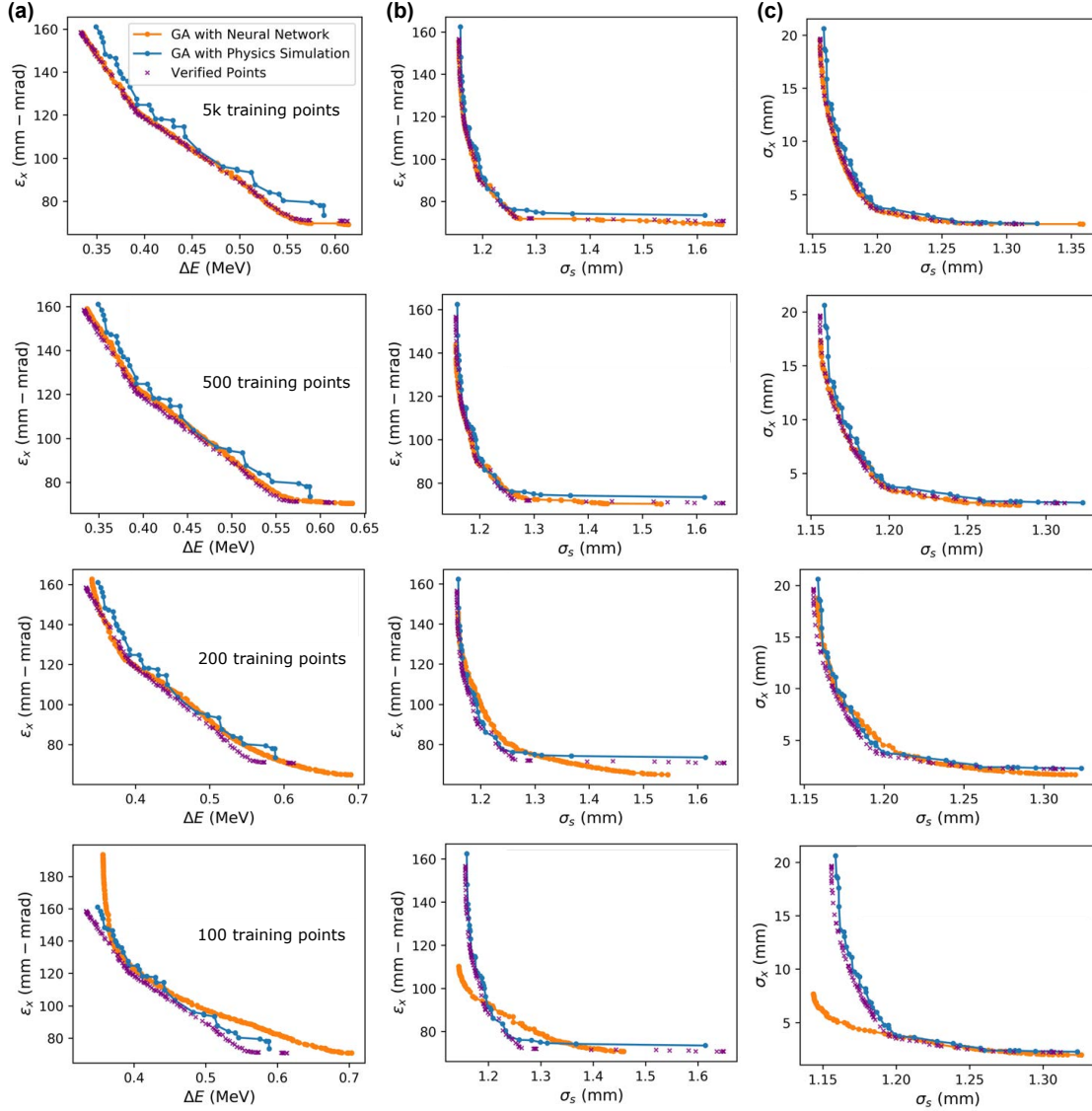


Figure 6: Impact of training sample size on quality of the Pareto front solutions. We show a comparison between Pareto fronts obtained from the NN for three sets parameters in the 40nC case: ΔE vs. ε_x (a), σ_z vs ε_x (b), and σ_z vs σ_x (c). Cases with 5k, 500, 200, and 100 training points are shown from top to bottom. 500 randomly-sampled training points are sufficient in this case for obtaining an accurate Pareto front with the NN model. For 200 training points, the Pareto front is quite a bit less accurate but still could provide an initial population for subsequent fine-tuning with a GA run on the physics simulation.¹⁷

Comparison with Different ML Models As a check to see whether a linear model would be sufficient for this problem, we trained a support vector regression (SVR) model³⁴ with a linear kernel. The mean squared error over all predicted beam parameters using the SVR model was 5.5×10^{-6} , in comparison to 3.5×10^{-10} for the NN model, indicating that we do gain accuracy by using a nonlinear model.

We also compared performance of NN and PCE surrogate models, both in parameter prediction and in the context of optimization. In Fig. 7, we show a comparison between the Pareto fronts obtained with the PCE and the NN models. The PCE mean squared error for 40 nC was 1.6×10^{-7} and for 1 nC was 4.5×10^{-6} . In contrast, the NN models were more accurate with a mean squared error of 3.5×10^{-10} and 2.9×10^{-8} on the 40 nC and 1 nC cases, respectively. However, one downside of using a simple NN model is that it does not inherently give an estimate of prediction uncertainty and model sensitivity without additional analysis. In contrast, the PCE model has the benefit of providing straightforward estimates of prediction uncertainty and sensitivity via the Sobol' indices^{23,35}. The PCE model also has fewer hyperparameters to tune (i.e., polynomial order, type of polynomial used).

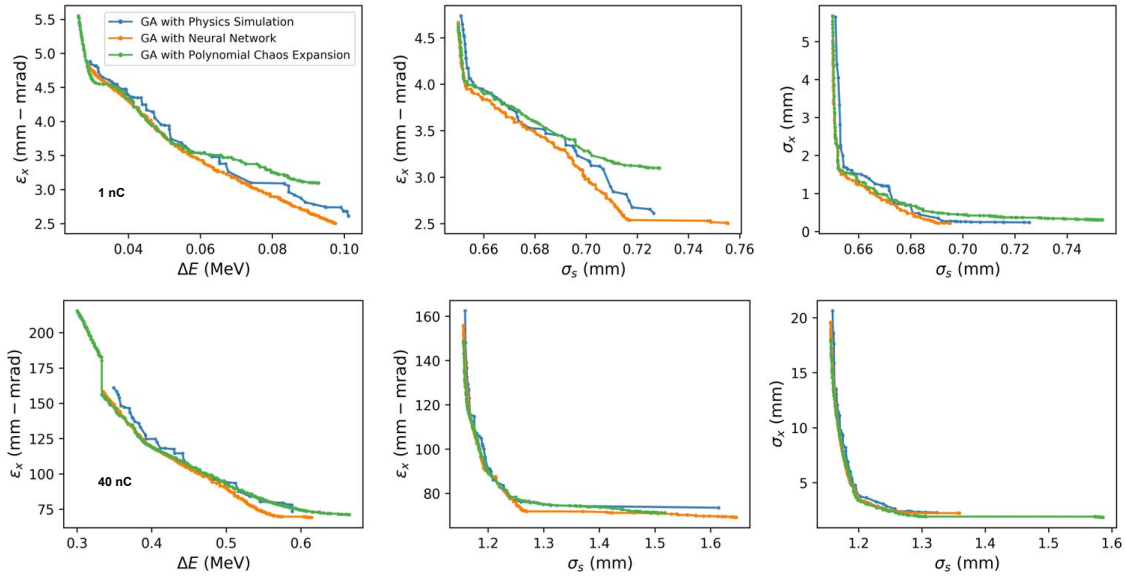


Figure 7: Pareto front comparisons for the PCE model and a NN model. In this case, 42,000 random sample points are used in training. Note that although the PCE model does not perform as well, it is more straightforward to train, has fewer hyperparameters to tune, and can be used to provide an uncertainty estimate. Although the fronts are less accurate, the points could be used as an initial starting point for a subsequent GA run on the physics simulation.

Extension to a Challenging Cyclotron Example

To assess this approach further, we applied it to a higher-dimensional and more complex accelerator problem: the IsoDAR cyclotron, shown in Fig. 8. The IsoDAR cyclotron will provide 60 MeV protons for sterile neutrino search ²⁶. It has also been proposed to use this machine to produce medical isotopes with high efficiency ³⁶. In all high-power proton machines, a major challenge is to minimize the number of uncontrolled, lost particles (thus maximizing the number that are sent to the relevant experiment and also minimizing damage to the machine). An indication for losses are large halos around the core of the particle beam. The halo can be quantified by a set of halo parameters and is proportional to the kurtosis, which is a measure of the “tailedness” of the probability distribution. A detailed description of this problem can be found in ²³.

The IsoDAR cyclotron simulation is an order of magnitude more expensive to evaluate than the AWA. This is due to the long path the particles travel, which results in a long integration time. We also attempt to predict a more difficult set of beam parameters than we did for the AWA. The most difficult parameter to predict is the beam halo, which is notoriously challenging to simulate accurately. Because the simulation is so computationally intensive, we use only a small number N of particles (i.e., $N = 1.33 \times 10^5$). As a result, we expect that the actual prediction of the halo is not fully converged.

Using a 2500-point random sample, we trained a NN to predict 12 beam parameter outputs: the number of lost particles (P_L), the beam energy (E), energy spread (ΔE), transverse and longitudinal beam sizes ($\sigma_x, \sigma_y, \sigma_s$), transverse and longitudinal emittances ($\varepsilon_x, \varepsilon_y, \varepsilon_s$), and the beam

halo (h_x, h_y, h_z). The 5 input parameters are the initial proton beam current and the positions of four families of collimators (corresponding to 16 collimators in total). For the GA run with the NN, we use 1000 generations with 300 individuals. Other than this, the implementation is exactly the same as that used for the AWA.

As expected, we find that the Pareto front predictions (see Fig. 9) are not as accurate as for the AWA. However, the points still roughly map out the region of parameter space near the Pareto front. It is unclear how much of this is a contribution from the simulation itself, which has not been tuned to ensure that the mesh size and number of particles is sufficient to produce a physically reliable result. Fine tuning of the simulation was not conducted because the associated computational intensity of the process for the broad range of parameters we are varying is too high. Note also that in this case we were unable to run a GA with the physics simulation because of the computational complexity and difficulty of convergence. All this taken into account, we consider being in close proximity to the Pareto front a successful use of the approach.

For the tradeoff between halo parameters and losses, we obtain better results when we produce a model that only predicts those direct outputs (as opposed to predicting and then optimizing all 12 objectives). In Fig. 9, we show this for h_x and P_L . This is also more in line with how GAs are typically used by accelerator physicists at present: often, only one or two important parameters will be optimized as competing objectives. We also find that by re-training the model with the verified points and repeating the process with the new model, we obtain a model that fills out more of the front (also shown in Fig. 9).

In addition, we also obtain a surrogate model that is $\mathcal{O}(10^7)\times$ faster to execute than the original physics simulation and can predict the 12 beam parameter outputs with reasonable accuracy (see Supplemental Material for a comparison of predictions on the test set, rather than predictions from model optimization).

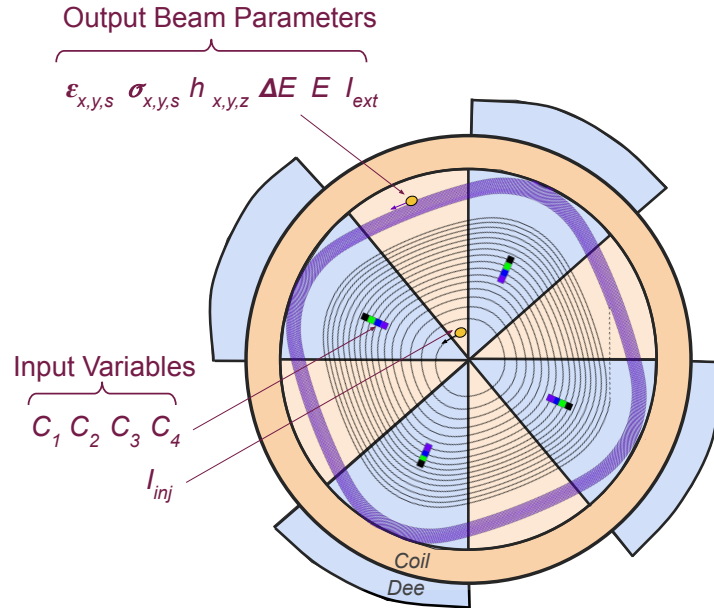


Figure 8: The IsoDAR schematic shown as an overlay of the magnetic field configuration (coil & dee) and central particle trajectories from the simulation. The radio frequency system used for acceleration is not shown. In black, the centroid trajectories of 18 turns are shown. A particle bunch of intensity I_{inj} is injected at the centre and passes through 4 families of collimators (indicated with the colored rectangles starting at turn 6). Each collimator family has one parameter $C_1 \dots C_4$ defining the collimator aperture. The collimator aperture and the initial intensity are input variables used by the optimizer. In this schematic, the extraction system is not shown, nor are all 100 turns of the beam. The last 10 turns before extraction are indicated in purple, together with the output beam parameters: the halo parameters $h_{x,y,z}$, the beam size $\sigma_{x,y,s}$, the projected emittance $\epsilon_{x,y,s}$ and the extracted beam current I_{ext} . Particle losses ($I_{inj} - I_{ext}$) in the collimators have to be minimized, but at the same time a small h_x is desired. This is one of the most important considerations in the design phase.

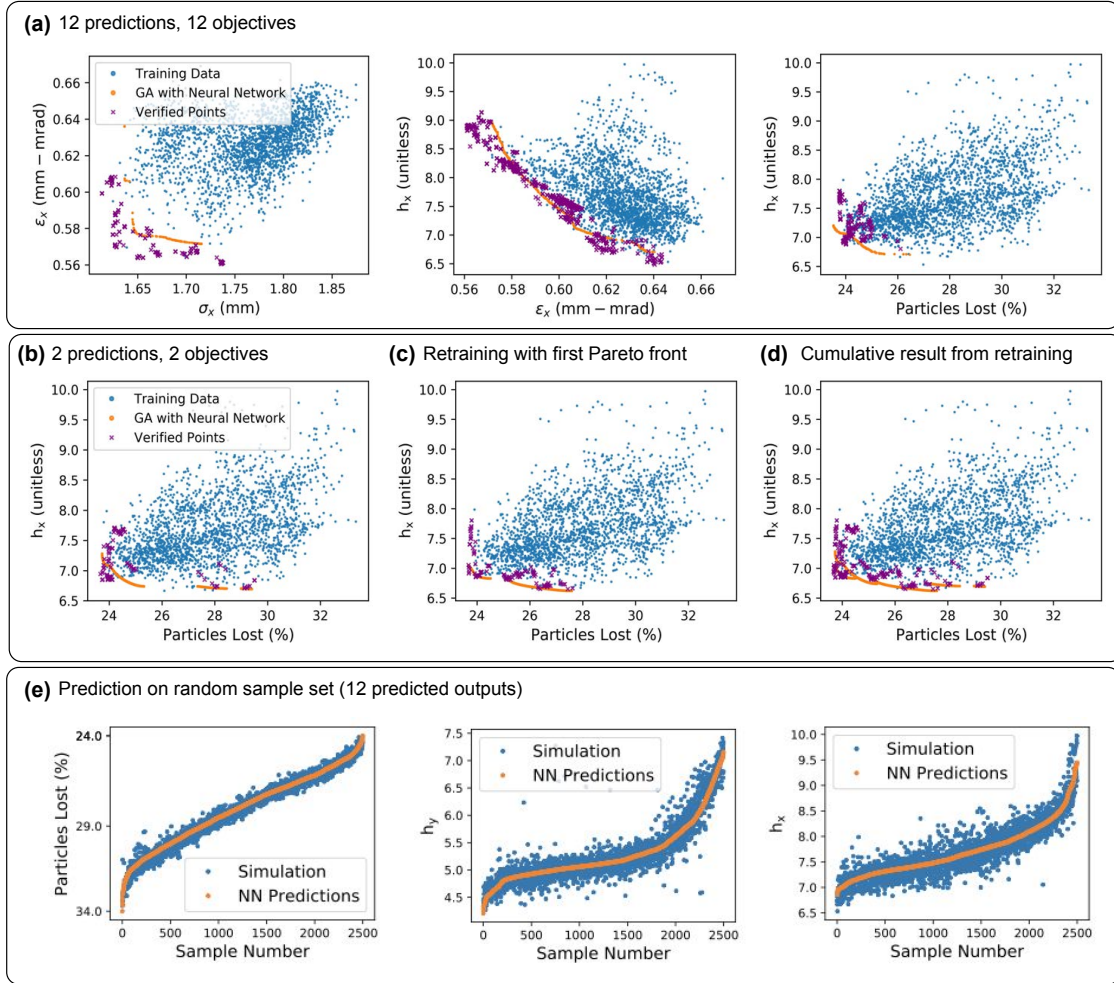


Figure 9: Example of Pareto fronts from IsoDAR NN model and corresponding verified points from the physics simulation. We first show results from training a model to predict and optimize 12 beam parameter outputs (a). We then show corresponding results from training only on the two most challenging beam parameter outputs, h_x and P_L (b). We then include the verified front from the previous model included the training set, retrain the model, repeat the optimization, and check the new Pareto points (c). Although the fronts do not match as well as they do for the AWA, for this challenging problem it is encouraging that we can predict roughly accurate fronts. Finally, we show the prediction on sorted values of the random sample set.

Discussion

In practice, physics simulations of particle accelerators are often too computationally expensive for full exploration of the parameter input space during optimization. The computational expense also limits (and in many cases prohibits) their use during machine operation to aid in prediction and control. In this work, we have shown that machine learning can be used to obtain a fast-executing representation of computationally intensive accelerator physics simulations, and that these models can be reliably used in multi-objective optimization using GAs. We have also shown that in some cases relatively little data is needed to achieve a high degree of fidelity relative to the original physics simulation. The ML models are more accurate than the simplified physics models that are presently used when fast execution is needed (e.g., fast envelope codes, simple tracking codes used with a small number of particles, etc). The ML approach thus provides one avenue toward creating fast-executing representations of high-fidelity physics simulations for use in machine operation, which would not otherwise be possible. It also enables faster start-to-end optimization, which could in turn help facilitate more thorough design optimization and experiment planning for these systems.

In addition, this technique requires substantially fewer simulation evaluations than a purely simulation-based optimization (e.g., $132\times$ fewer simulations in the case of the AWA). This opens up the possibility to do more extensive optimization than might otherwise have been feasible using computationally intensive physics simulations alone, both for new designs and for experiment planning. Assuming the physical function to be modeled is smooth and that the NN is learning a

good representation of the underlying physical system, running the GA with the ML model can provide an estimate of the Pareto front in a fraction of the time needed to run the GA on the physics model. The computational cost of the parameter space exploration with the GA before it gets close to convergence is high, and using the ML model effectively enables one to skip these early stages of convergence and form a model that can be used to interpolate across the input and output space. In addition, a larger generation and population size can be used with the NN than would normally be feasible with the physics simulation, thus potentially enabling better solutions to be found. Ultimately, using the NN to aid the optimization process could be useful in cases where one cannot in practice run a GA for a sufficient number of generations or with a large enough population to converge. This can be the case when HPC resources are limited and/or the optimization problem is too high-dimensional or computationally intensive.

For our study, we used a random sample of the physics simulation. However, in some cases accelerator scientists may already have samples available from prior GA and could use that data set directly to train the ML model. Since the GA has already been run, this is useful if the main goal is to obtain a fast-executing representation of the physics simulation.

Looking forward, several useful avenues for using this approach in particle accelerator applications are apparent:

First, one can begin to use these surrogate models directly in machine operation. In some cases, high-fidelity simulations have been made to match the machine very closely and can be used to provide suggested machine settings (for a comprehensive example, see ³⁷). If the simulation

matches the machine closely enough, the ML model trained on the simulations can immediately be used to aid operation. Such models could aid machine operation by including them in model-based control and optimization routines (e.g., using the model to help guide the search for optimal settings). Machine operators could check the potential impact of setting changes before trying them out on the actual machine. These models could also be used as a diagnostic tool to provide predictions about un-measured beam parameters (i.e., a virtual diagnostic ^{20,38}) or to flag when the system has changed substantially (i.e., anomaly/failure detection). Finally, calibrated inputs from the machine and subsequent online optimization of the model can be used to provide a warm start to a local, feedback-based optimization algorithm. This is similar to the warm start approach described and tested in ³⁹, but it uses optimization around the forward model to obtain the initial suggested settings rather than using an inverse model. The advantage of such combined approaches is that they help compensate for inevitable discrepancies between the model and the machine (e.g., due to drift, hidden variables, etc.); the suggested settings from the model only need to be close enough to the basin of a good minimum to allow the local optimizer to converge.

Second, getting the physics simulation to match the measured machine behavior can be very difficult and usually requires substantial effort, and this becomes more acute for larger and more complex accelerator systems. As a result, many accelerator facilities do not prioritize creating accurate physics simulations (particularly since the high-fidelity physics simulation cannot be used directly in operation anyway, at least prior to the introduction of the approach discussed in this paper). With the surrogate model, one can instead update the model learned in simulation with measurements from the machine to account for deviations between the simulation and the real

machine behavior. This was shown to be viable in ²⁰, but more rigorous study is needed to address the impact of machine drift and develop effective strategies for model retraining over time.

Third, a model that supports uncertainty quantification is advantageous when considering how these models may be used in design and online optimization of the running accelerator. For example, one might want an uncertainty estimate on an output parameter. The input-output relationships in real accelerators are also subject to noise (including heteroscedastic noise), drift over time, and the influence of unobserved variables. Using expressive models that also include uncertainty estimates (e.g., Bayesian Neural Networks) is a reasonable next step. Although we do not include them here, Gaussian Processes models also provide uncertainty predictions and have been used in Bayesian optimization of operational accelerators ⁴⁰⁻⁴². This kind of optimization could also be used in tandem with sampling the simulation parameter space more efficiently to produce a good surrogate model (e.g., in our case with a random sample of the inputs, the output space is not sampled evenly).

Finally, our results suggest a new procedure for doing GA optimization of particle accelerators. Instead of running a GA with a physics simulation, one can run a small random sample over the parameter space, train a surrogate model on this small sample, and run a full GA using the surrogate model very quickly. Then the Pareto points obtained from the surrogate model can be used as an initial population in a subsequent short GA with the physics simulation to verify and fine-tune the result (see Fig. 10). This could also be repeated until convergence to a good solution is reached. While training the NN as an intermediate step in the optimization process may seem

cumbersome, GAs do have their own hyperparameters that need to be tuned (e.g., population size, number of generations, crossover and mutation probabilities). The risk of wasting computational resources while tuning these parameters is high, and in practice accelerator physicists often just pick a number of generations to run based on experience. Some of these could instead be initially tuned with the ML model to potentially save some computational resources.

How this approach will scale to accelerator systems with a greater number of input/output variables, wider ranges of variables, or more complex beam dynamics will be addressed in future work. Injector systems that are similar in scale and complexity to the AWA are extremely common, and these results should provide good guidance for those wishing to use this method on similar components. The fact that we used a similar neural network architecture to other injector modeling problems also hints at the possibility of doing transfer learning between models (e.g., training on one injector system and then re-using the model with small updates for a similar injector system). While the IsoDAR is a more unique design, the performance of the ML approach on that case shows it can be used in cases with much more complicated beam dynamics. As many beam dynamics problems in accelerators are similar, it is also reasonable to expect that these results could provide good starting points for applying this approach to other kinds of accelerator systems.



Figure 10: Workflow for a method to obtain orders of magnitude faster GA optimization of particle accelerators. First, run a small random sample of inputs through the physics simulation (e.g., a few hundred points in our case) (a). Train an ML model on the random sample (b). Run the GA with the ML model to obtain predictions of the Pareto front and corresponding optimal input settings on the machine (c). Use the predicted optimal input settings as the initial population in a second, shorter GA optimization over the physics simulation to fine-tune the result (d). One can also incorporate the new data into a second training of the ML model and repeat these steps as needed until convergence.

Methods

Data Sets for the Surrogate Models We generated uniformly-distributed random samples from the physics simulation. For this we used the OPAL-based interface for creating such data sets, which was developed in part to support this effort. This feature allows the submission of massively parallel jobs using an OPAL input file.

For the AWA, the randomly-varied inputs include the injector phase ϕ_1 and gradient G_1 , the linac cavity phase ϕ_2 and gradient G_2 , and two solenoid strengths K_1 and K_2 . The output parameters are the transverse spot sizes σ_x and σ_y , the longitudinal beam size σ_s , the transverse projected emittances values ε_x and ε_y , the longitudinal projected emittance ε_s , and the energy spread ΔE . The input variable ranges are informed by the operating ranges at the AWA (see Table 3). Random samples for two bunch charges were generated (1 nC and 40 nC, with the corresponding laser radius being 2 mm and 9 mm). In the 1 nC case, we generated 70k samples, and in the 40 nC case, we generated 80k samples. However, we only use a small subset of these during training of the models.

For the IsoDAR cyclotron, the input parameters varied are the initial beam current I_{inj} and four collimator settings $C_1 - C_4$. The ranges of the collimators and the beam current are determined by technical design considerations. A random sample of 2500 points was generated for the initial training data set. For retraining, 100 points from the previous Pareto front were selected randomly to add to the training set.

The implementation of NSGA-II³⁰ that is provided within OPAL was used for the GA with the physics simulation of the AWA. Details related to the algorithm can be found in⁴³. The implementation of the GA used with OPAL is slightly different than the implementation in DEAP (used with the ML models) because some of the adjustable hyperparameters are defined differently. However, when comparing the two algorithms on OPAL simulations of the AWA, the fronts produced

Name	Abbreviation	Min Value	Max Value	Unit
Solenoid 1 Strength	K_1	400	550	m^{-1}
Solenoid 2 Strength	K_2	180	280	m^{-1}
Injector Phase	ϕ_1	-10	0	deg
Cavity Phase	ϕ_2	-10	0	deg
Injector Accelerating Gradient	G_1	60	75	MVm^{-1}
Cavity Accelerating Gradient	G_2	15	25	MVm^{-1}

Table 2: Range of the AWA Input Variables.

Name	Abbreviation	Min Value	Max Value	Unit
Initial Beam Current	I_{inj}	5.5	7.5	mA
Collimator 1	C_1	2.37	2.63	unitless
Collimator 2	C_2	2.37	2.63	unitless
Collimator 3	C_3	7.60	8.40	unitless
Collimator 4	C_4	7.60	8.40	unitless

Table 3: Range of the IsoDAR Input Variables.

by each method are in reasonable agreement. We choose an initial population of 656 individuals and subsequently evolve the population over 200 generations, while retaining the same number of individuals in each generation. The following hyper-parameters were used: gene mutation probability $P_g = 0.8$, mutation probability $P_m = 0.8$, and recombination probability $P_r = 0.2$. Specific descriptions of the hyperparameters can be found in Section 1.4.2 of the OPAL manual ⁴⁴. The specific values used in this case were chosen based on previous optimization work for the AWA that involved a hyperparameter scan ⁵. The constraints of the MOO problem were set such that the variables stayed within the operating ranges of the AWA (see Table 3). For each generation, the input and output parameters from the simulation are saved. In the 1 nC and 40 nC cases respectively, 59,285 and 65,929 final samples were obtained. See Table 4 for an overview of the computational resources required to make the physics simulation data sets. For the IsoDAR cyclotron, no GA was run on the physics simulation due to the computational expense and difficulty obtaining convergence.

OPAL Simulation OPAL is an open-source, parallel library for electrostatic PIC simulations of charged particle accelerators. More details can be found in the OPAL manual (see ⁴⁴). For simulations of the AWA, 3D space charge forces are calculated throughout the time-evolution of the beam, which is important for realistically capturing the nonlinear impact of the beam self-fields. The particle generation at the CsTe photo-cathode is modeled using an uniform emission model, assuming a planar ideal surface. The laser profile used for emission is uniform transversely and a flattop longitudinally, with Gaussian tails. Convergence studies were previous done to determine an appropriate time step, mesh size, and number of particles to use (here, 1×10^{-11} seconds for

the time step, $16 \times 16 \times 32$ grid cells for the space charge mesh, and 10k macro-particles). The full-width-half-maximum of the laser in the longitudinal direction was 6 ps for both cases. The laser radius was set to 2 mm for the 1 nC simulations. Due to large nonlinear space charge forces at 40 nC, the laser radius was increased to 9 mm. These are typical operating conditions at the AWA.

Field maps generated in POISSON⁴⁵ were used to model the solenoid magnets. Two types of rf field maps were used to model the gun and accelerating cavities. 2D maps were generated in SUPERFISH⁴⁶ and used in the 1 nC case. 3D maps were generated in ACE3P⁴⁷ and used in the

Case	Calculation	Core-hours	Wall time (hours)	Sim. evals.
AWA 1 nC	Genetic Algorithm (200 gen)	43,500	16.56	65,929
	Random Sample	60,600	4.12	70,000
	500 points	283	0.14	500
AWA 40 nC	Genetic Algorithm (200 gen)	95,000	36	65,928
	Random Sample	115,700	7.23	80,000
	500 points	660	0.33	500
IsoDAR	Random Sample	13,335	1.7	2,500

Table 4: Overview of the data sets from the physics simulations and the computational resources used for generating them. Note that we found that to make accurate surrogate models we needed many fewer randomly sampled points than were initially generated. For the GAs, 2624 cores were used. For the 1nC random sample, 16k cores were used, and for the 40nC random sample, 15k cores were used.

40 nC simulations. While 3D field maps are computationally more expensive to evaluate, they are more accurate and capture asymmetries that are present in the AWA rf cavities.

The IsoDAR simulation is described in section II of ⁴⁸. In addition, in this work we added 4 collimators to clean up the beam (i.e., reduce halo). The collimators are placed in the central region of the cyclotron where the energy is low and the activation is negligible.

Implementation of Machine Learning Based Surrogate Models The NNs were implemented in Keras ⁴⁹, with TensorFlow ⁵⁰ as the backend. For general demonstration of the technique, we used a topology and set of hyperparameters that the authors had previously found to work well for similar problems in accelerators ²⁰⁻²². This consisted of a fully-connected, feed-forward NN with four hidden layers, each with 20 nodes and hyperbolic tangent activation functions. No regularization penalties (e.g., L_1 or L_2 norm) were used on the weights. The NNs were trained for 10k epochs with a batch size of 500 points. The Adam optimization algorithm ⁵¹ was used for training, with an initial learning rate of 0.001 and hyperparameters $\beta_1 = 0.9$, and $\beta_2 = 0.999$. For training, the random sample data was randomly split into training (60%), validation (20%), and testing (20%) sets. All data sets were scaled to fit within an appropriate range. For example, in our case the data was scaled to be within the range of $[-1, 1]$. For the IsoDAR problem, the setup is the same, except we use a neural network with a slightly different number of nodes in each hidden layer: 10 – 20 – 20 – 15 nodes in each layer respectively.

The surrogate model based on polynomial chaos expansion (PCE) is constructed using the Uncertainty Quantification Toolkit (UQtk) ⁵². This library provides functionalities to perform an

intrusive as well as a non-intrusive UQ in C++ and Python. In contrast to the projection method of ²³, we used the regression method ^{53,54} with Legendre polynomials, and we associate a uniform distribution to all input variables. In this work, we closely follow ²³ in regard to the PCE surrogate model. Furthermore, choosing a polynomial order of $p = 4$ and 60% of the random sample for training matches the performance of the NN model most closely.

The GA optimization with the surrogate models is done using the Python package DEAP ⁵⁵ and its standard implementation of NSGA-II. We picked hyperparameters that were as close as possible to those used with the OPAL GA.

Code Availability For this research only open source software is used. This includes the accelerator simulation framework OPAL ⁴⁴ and Python-based software tools: DEAP ⁵⁵, Keras ⁴⁹, TensorFlow ⁵⁰, UQtk ⁵², and sci-kit learn ⁵⁶.

1. Mitchell, M. *An Introduction to Genetic Algorithms* (MIT Press, Cambridge, MA, USA, 1996).
2. Bäck, T. *Evolutionary Algorithms in Theory and Practice: Evolution Strategies, Evolutionary Programming, Genetic Algorithms* (Oxford University Press, Inc., New York, NY, USA, 1996).
3. Bazarov, I. V. & Sinclair, C. K. Multivariate optimization of a high brightness dc gun photoinjector. *Phys. Rev. ST Accel. Beams* **8**, 034202 (2005).

4. Hofler, A. *et al.* Innovative applications of genetic algorithms to problems in accelerator physics. *Phys. Rev. ST Accel. Beams* **16**, 010101 (2013).
5. N. Neveu *et al.* Parallel general purpose multiobjective optimization framework with application to electron beam dynamics. *Phys. Rev. Accel. Beams* **22**, 054602 (2019). URL <https://link.aps.org/doi/10.1103/PhysRevAccelBeams.22.054602>.
6. Chu, C. *et al.* XAL-based applications and online model for LCLS. In *Proc. of PAC*, FR5REP022 (2010).
7. Pelaia, T. Open XAL Status Report 2013. In *Proc. of IPAC*, MOPWO086 (2013).
8. Scheinker, A. & Gessner, S. Adaptive method for electron bunch profile prediction. *Phys. Rev. ST Accel. Beams* **18**, 102801 (2015).
9. Ryne, R. *et al.* Scidac advances and applications in computational beam dynamics. *J. Phys. Conf. Ser.* **16**, 210 (2005).
10. SciDAC: Scientific Discovery through Advanced Computing. URL <https://scidac.gov/>.
11. Adelman, A., Locans, U. & Suter, A. The dynamic kernel scheduler - part 1. *Comput. Phys. Commun.* **207**, 83–90 (2016).
12. Borland, M. Elegant: A flexible sdds-compliant code for accelerator simulation. Tech. Rep. LS-287, Argonne National Laboratory (2000-2018).

13. Takeda, H. & Stovall, J. E. Modified parmila code for new accelerating structures. In *Proc. of PAC*, vol. 4, 2364–2366 (1995).
14. Baily, S. A., Pang, X. & Rybarcyk, L. High-performance beam simulator for the lansa ce linac. In *Proc. of IPAC*, C1205201 (2012).
15. Sun, Y. Multi-Objective Online Optimization of Beam Lifetime at APS. In *Proc. of NAPAC*, WEPOB12 (2017).
16. Bergan, W. F. *et al.* Online storage ring optimization using dimension-reduction and genetic algorithms. Preprint at <https://arxiv.org/abs/1807.10720> (2018).
17. Vay, J.-L. Noninvariance of space- and time-scale ranges under a lorentz transformation and the implications for the study of relativistic interactions. *Phys. Rev. Lett.* **98**, 130405 (2007).
18. Vay, J.-L., Haber, I. & Godfrey, B. B. A domain decomposition method for pseudo-spectral electromagnetic simulations of plasmas. *Journal of Computational Physics* **243**, 260 – 268 (2013).
19. Lehe, R., Kirchen, M., Andriyash, I. A., Godfrey, B. B. & Vay, J.-L. A spectral, quasi-cylindrical and dispersion-free particle-in-cell algorithm. *Computer Physics Communications* **203**, 66 – 82 (2016).
20. Edelen, A., Biedron, S., Edelen, J. & Milton, S. First steps toward incorporating image based diagnostics into particle accelerator control systems using convolutional neural networks. In *Proc. of NAPAC*, TUPOA51 (2017).

21. Edelen, A., Edelen, J., Biedron, S., Milton, S. & van der Slot, P. Using a neural network control policy for rapid switching between beam parameters in a FEL. In *Proc. of IFEL*, 406–409 (2017).
22. Edelen, A., Edelen, J., Biedron, S., Milton, S. & van der Slot, P. Recent Applications of Neural Networks to Modeling and Control of Particle Accelerators. In *Proc. of IPAC, THYGBE2* (2018).
23. Adelman, A. On nonintrusive uncertainty quantification and surrogate model construction in particle accelerator modeling. *SIAM/ASA Journal on Uncertainty Quantification* **7**, 383–416 (2019). <https://doi.org/10.1137/16M1061928>.
24. Edelen, A. *et al.* Opportunities in Machine Learning for Particle Accelerators. *White paper from the 1st ICFA Machine Learning Workshop for Particle Accelerators*. Preprint at <https://arxiv.org/abs/1811.03172> (2018).
25. Conde, M. *et al.* Research program and recent results at the argonne wakefield accelerator facility (AWA). In *Proc. of IPAC, WEPAB132* (2017).
26. Bungau, A. *et al.* Multivariate optimization of a high brightness dc gun photoinjector. *Phys. Rev. Lett.* **109**, 141802 (2012).
27. Meiss, J. *Rev. Mod. Phys.* **64**, 795–848 (1992).
28. Pang, X. & Rybarcyk, L. Multi-objective particle swarm and genetic algorithm for the optimization of the LANSCE linac operation. *NIM A.* **741**, 124–129 (2014).

29. Kennedy, J. & Eberhart, R. Particle swarm optimization. *Proc. of ICNN'95 - International Conference on Neural Networks*. (1995).
30. Deb, K., Pratap, A., Agarwal, S. & Meyarivan, T. A fast and elitist multiobjective genetic algorithm: NSGA-II. *IEEE Trans. Evol. Comput.* **6**, 182–197 (2002).
31. Ha, G. *et al.* Perturbation-minimized triangular bunch for high-transformer ratio using a double dogleg emittance exchange beam line. *Phys. Rev. Accel. Beams* **19**, 121301 (2016).
32. Gai, W., Power, J. G. & Jing, C. Short-pulse dielectric two-beam acceleration. *J. Plasma Phys.* **78**, 339345 (2012).
33. Smith, R. *Uncertainty Quantification: Theory, Implementation, and Applications* (SIAM, 2014).
34. Vapnik, V. *Statistical learning theory*. Adaptive and learning systems for signal processing, communications, and control (Wiley, 1998).
35. Sobol, I. Global sensitivity indices for nonlinear mathematical models and their monte carlo estimates. *Mathematics and Computers in Simulation* **55**, 271 – 280 (2001).
36. Alonso, J. R. *et al.* Medical isotope production with the IsoDAR cyclotron. *Nature Reviews Physics*. (2019).
37. Gulliford, C. *et al.* Demonstration of low emittance in the cornell energy recovery linac injector prototype. *Phys. Rev. ST Accel. Beams* **16**, 073401 (2013).

38. Emma, C., Edelen, A. L. *et al.* Machine Learning Based Longitudinal Phase Space Prediction for Accelerators. *PRAB*. .
39. Scheinker, A., Edelen, A. L. *et al.* Model-independent tuning for maximizing free electron laser pulse energy. *PRAB*. .
40. McIntire, M., Cope, T., Ermon, S. & Ratner, D. Bayesian Optimization of FEL Performance at LCLS. *Proc. of IPAC. WEPOW055* (2016).
41. McIntire, M., Ratner, D. & Ermon, S. Sparse Gaussian processes for Bayesian optimization. *UAI'16 Proceedings of the Thirty-Second Conference on Uncertainty in Artificial Intelligence*. 517–526 (2016). <https://www-cs.stanford.edu/~ermon/papers/sparse-gp-uai.pdf>.
42. Johannes, K., Mutny, M., Hiller, N., Ischebeck, R. & Krause, A. Adaptive and Safe Bayesian Optimization in High Dimensions via One-Dimensional Subspaces. *UAI'16 Proceedings of the Thirty-Second Conference on Uncertainty in Artificial Intelligence*. (2019). <https://arxiv.org/pdf/1902.03229.pdf>.
43. Ineichen, Y. *Toward massively parallel multi-objective optimization with application to particle accelerators*. Ph.D. thesis, ETH Diss. 21114 (2013).
44. Adelman, A. *et al.* The OPAL (Object Oriented Parallel Accelerator Library) Framework. Tech. Rep. PSI-PR-08-02, Paul Scherrer Institut (2008-2019).

45. Warren, J. L., Boicourt, G. P., Menzel, M. T., Rodenz, G. W. & Vasquez, M. C. Revision of and Documentation for the Standard Version of the POISSON Group Codes. *IEEE Trans. Nucl. Sci.* **32**, 2870–2872 (1985).
46. Halbach, K. & Holsinger, R. F. Superfish-a computer program for evaluation of rf cavities with cylindrical symmetry. *Part. Accel.* **7**, 213–222 (1976).
47. Kononenko, O. *et al.* Advances in massively parallel electromagnetic simulation suite ACE3P. In *Proc. of ICAP, FRAJ13* (2016).
48. Yang, J. *et al.* Beam Dynamics Simulation for the High Intensity DAEdALUS Cyclotrons. *NIM A* 84–91 (2013).
49. Chollet, F. *et al.* Keras: The python deep learning library (2015).
50. Abadi, M. *et al.* TensorFlow: Large-scale machine learning on heterogeneous systems (2015).
51. Kingma, D. P. & Ba, J. Adam: A method for stochastic optimization. *CoRR*. Preprint at <https://arxiv.org/abs/1412.6980> (2014).
52. Debusschere, B., Sargsyan, K., Safta, C. & Chowdhary, K. *Uncertainty Quantification Toolkit (UQtk)*, 1–21 (Springer International Publishing, Cham, 2016).
53. Debusschere, B. *et al.* Numerical challenges in the use of polynomial chaos representations for stochastic processes. *SIAM J. Sci. Comput.* **26**, 698–719 (2004).
54. Sudret, B. Global sensitivity analysis using polynomial chaos expansions. *Reliability Engineering & System Safety* **93**, 964 – 979 (2008).

55. Fortin, F.-A., De Rainville, F.-M., Gardner, M.-A., Parizeau, M. & Gagné, C. DEAP: Evolutionary algorithms made easy. *J. Mach. Learn. Res.* **13**, 2171–2175 (2012).
56. Pedregosa, F. *et al.* Scikit-learn: Machine learning in Python. *J. Mach. Learn. Res.* **12**, 2825–2830 (2011).

Acknowledgements We gratefully acknowledge the computing resources provided on Bebop, a high-performance computing cluster operated by the LCRC at ANL. The training of the surrogate models benefited from the ETH Leonard cluster the CSCS Piz-Daint, the PSI Merlin-6 and the SLAC OCIO Jupyter-Hub GPU cluster.

This work was supported by the U.S. Department of Energy, Office of Science, under contract numbers DE-AC02-76SF00515, DE-AC02-06CH11357, and grant number DE-SC0015479.

Competing Interests The authors declare that they have no competing financial interests.

Correspondence Correspondence and requests for materials should be addressed to A.E. (email: eden@slac.stanford.edu)